Electronic Supplementary Material (ESI) for Nanoscale

Tunable Pt nanocatalysts for the aerobic selox of cinnamyl alcohol

Lee J. Durndell,[a] Christopher M. A. Parlett,[a] Nicole S. Hondow,[b] Karen Wilson[a] and Adam F. Lee[a*]

[a] Cardiff Catalysis Institute, School of Chemistry, Cardiff University, Cardiff CF10 3AT, UK

[b] Institute for Materials Research, School of Process, Environmental and Materials Engineering, University of Leeds, Leeds, LS2 9JT, UK

Structural and catalytic properties of silicas and Pt/silicas

Parent silica supports

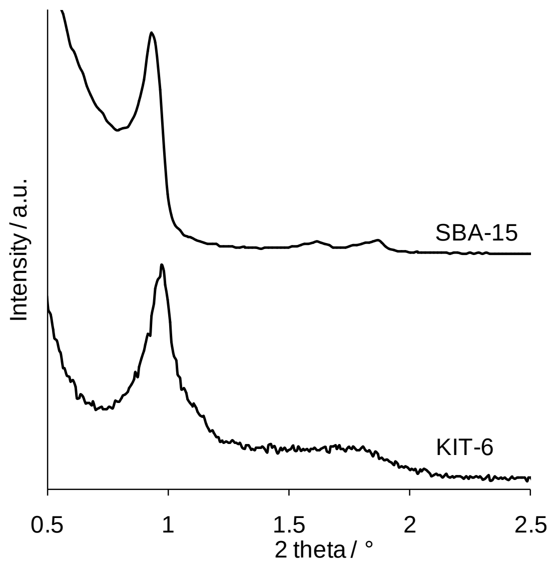

Figure S1. Low Angle XRD patterns for parent mesoporous silica supports.Offset for clarity.

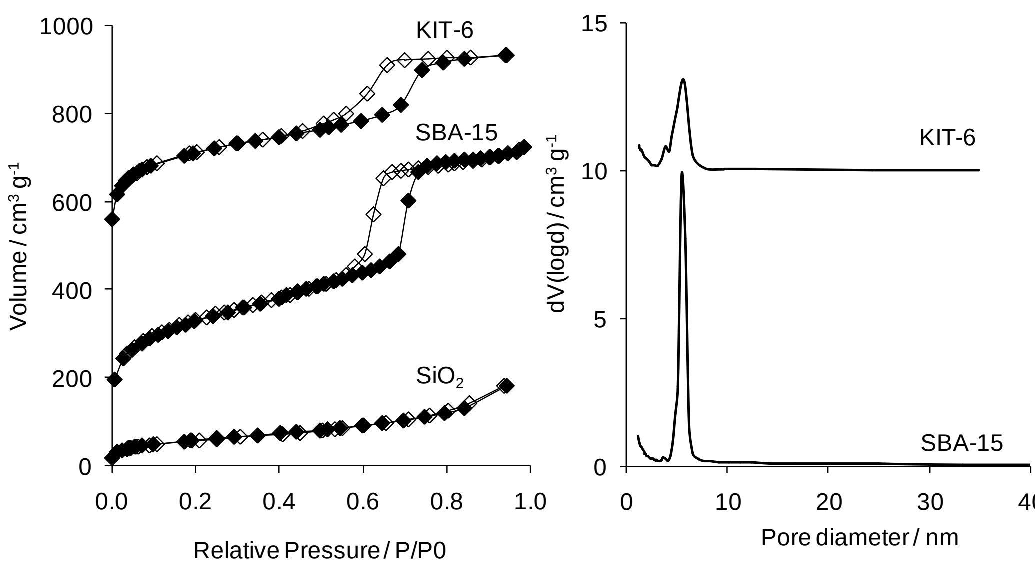

Figure S2. Nitrogen adsorption-desorption isotherms and associated BJH pore size distributions for parent mesoporous silica supports. Offset for clarity.

Table S1. Textural properties of parent silica supports

Sample	Surface area / $m^2 g^{-1(a)}$	Mesopore Diameter / $nm^{(b)}$	Lattice Parameter / $nm^{(c)}$	Pore Separation / $nm^{(c)}$
SiO_2 (S5505)	208.2	31.3	n/a	n/a
SBA-15	1031.9	5.8	9.0	10.4
KIT-6	1144.1	6.6	22.2	22.2

[a]N_2 BET, [b]BJH desorption isotherm, [c]Low angle XRD via Bragg's law

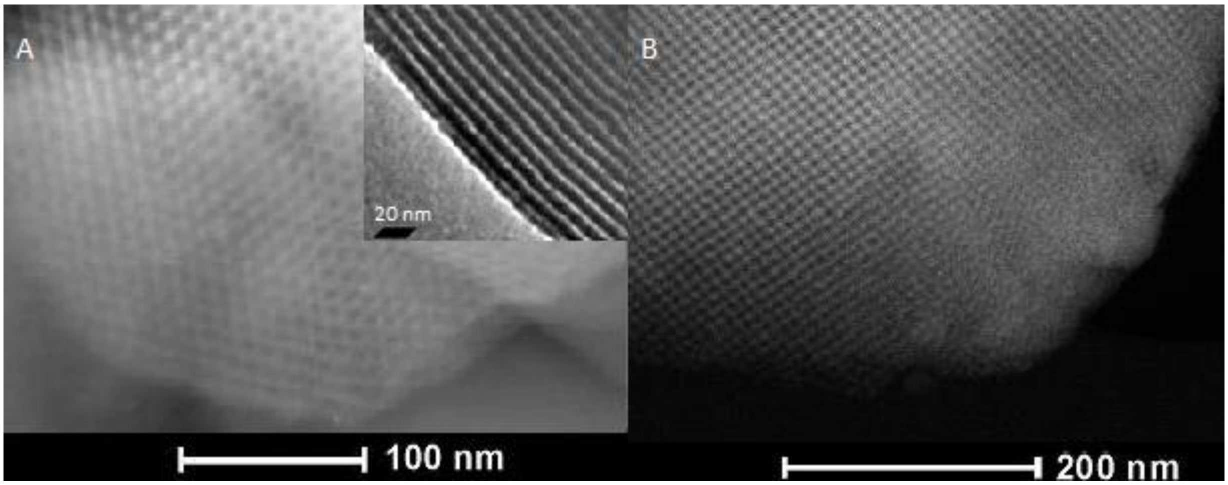

Figure S3a. High-resolution TEM (HRTEM) dark field images of parent (a) SBA-15 and (b) KIT-6 supports

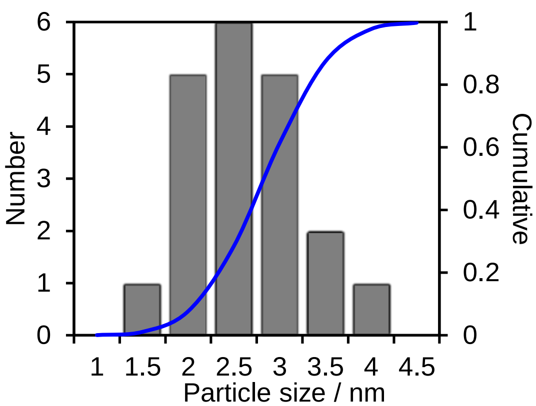

Figure S3b. HRTEM particle size distribution for 0.1 wt% Pt/SBA-15

Pt-impregnated silica supports

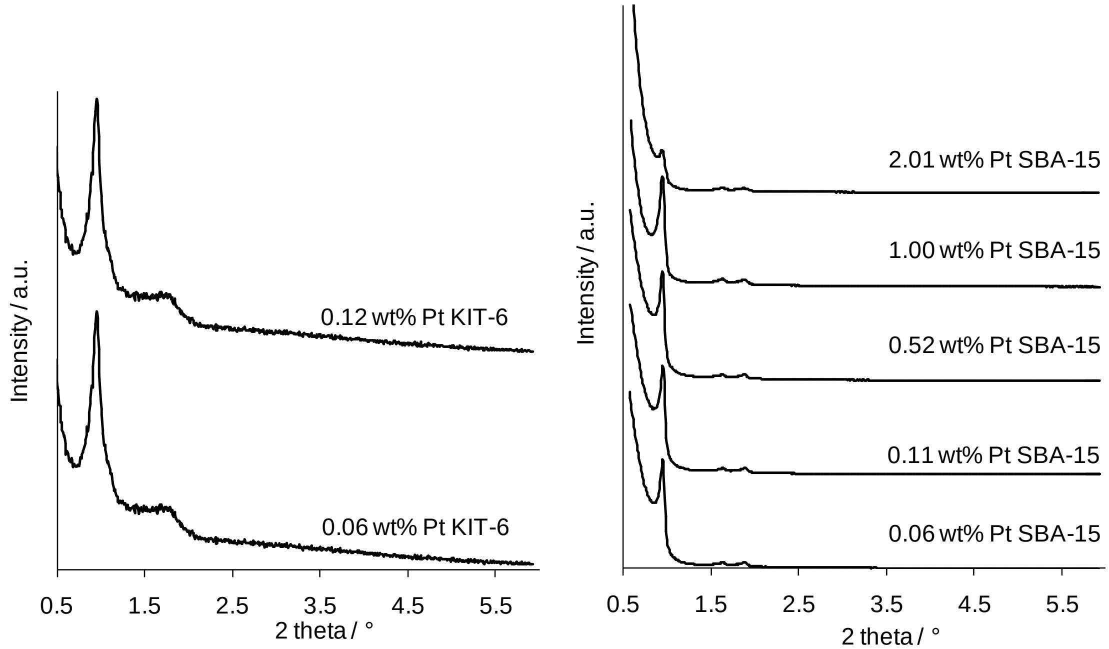

Figure S4. Low angle XRD for Pt-impregnated KIT-6 (left) and SBA-15 (right). Pore structure is preserved following impregnation. Offset for clarity.

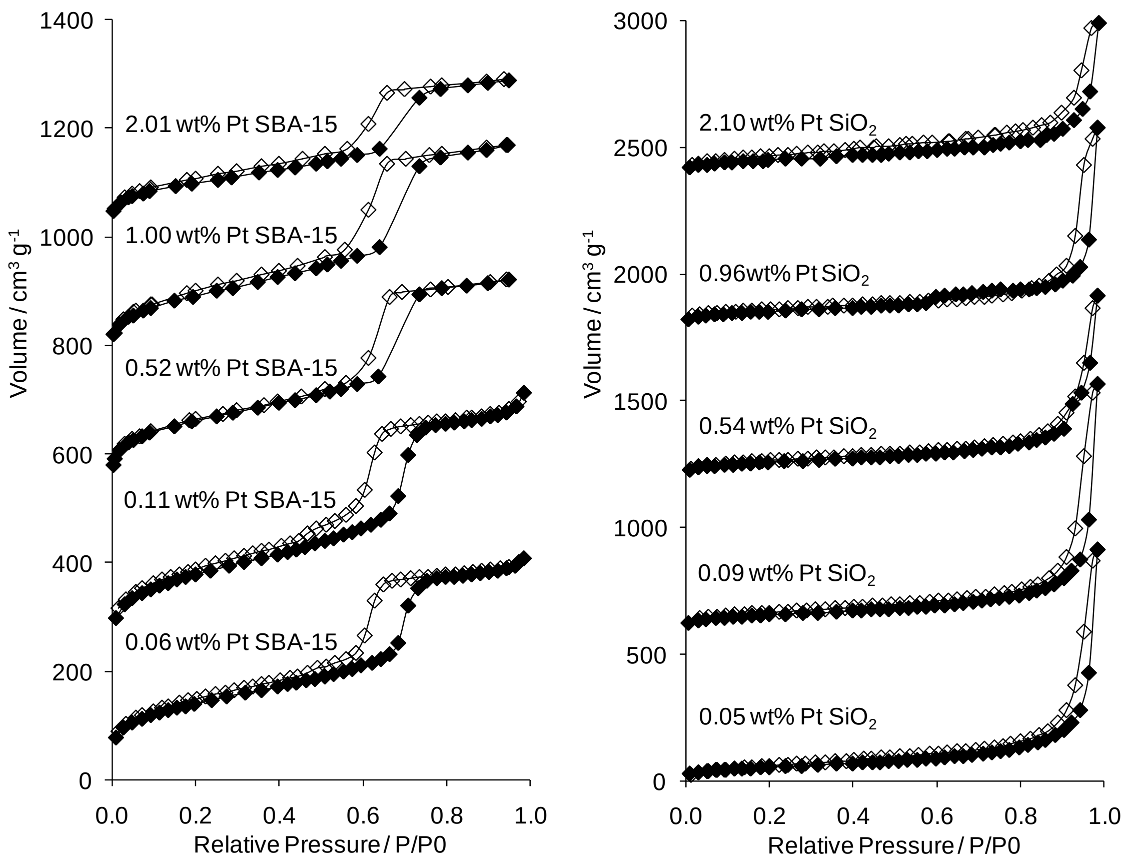

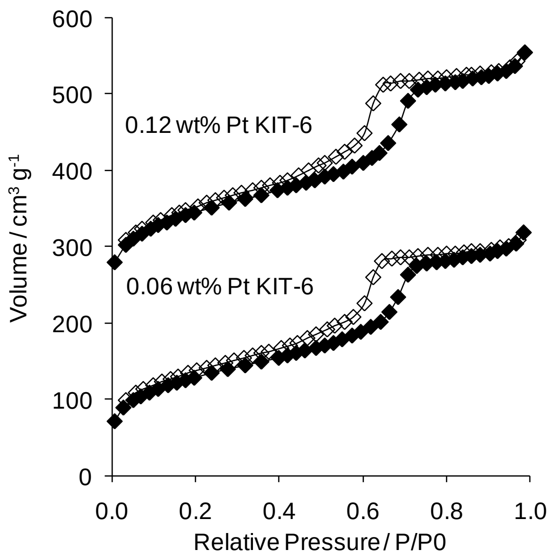

Figure S5. Nitrogen adsorption-desorption isotherms for Pt impregnated KIT-6 (bottom), SBA-15(top left) and commercial fumed silica (top right). Offset for clarity.

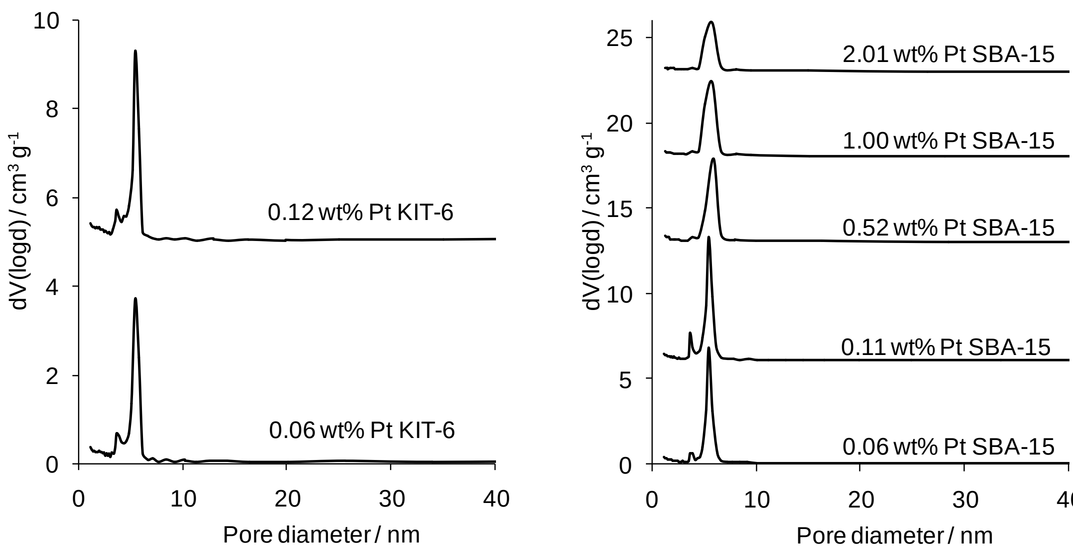

Figure S6. BJH pore size distributions for Pt impregnated KIT-6 (left) and SBA-15 (right). Offset for clarity.

Table S2. Physico-chemical properties of Pt/silicas

Support	Pt loading / wt%[(a)]	Pt dispersion / %[(b)]	Pt particle size / nm[(c)]	PtO_2 content / %[(d)]	Surface area / $m^2\ g^{-1}$[(e)]	Mesopore diameter / nm[(f)]
SiO_2	2.10	10.0	15.6 (16.6)	7.7	176.16	n/a
SiO_2	0.96	14.7	9.7 (9.5)	10.1	188.25	n/a
SiO_2	0.54	20.0	7.7 (8.4)	16.2	192.50	n/a
SiO_2	0.09	44.4	3.4	23.2	194.36	n/a
SiO_2	0.05	52.4	3.0	26.7	189.93	n/a
SBA-15	2.01	14.9	14.3 (15.1)	13.8	610.69	5.8
SBA-15	1.00	18.3	7.9 (9.0)	14.8	638.45	5.8
SBA-15	0.52	31.8	3.8 (5.4)	18.1	679.22	5.8
SBA-15	0.11	70.9	2.6	33.8	702.19	5.8
SBA-15	0.06	82.5	2.3	36.0	734.20	5.8
KIT-6	0.12	80.6	1.8	34.7	822.02	6.7
KIT-6	0.06	84.1	1.7	38.1	861.47	6.7

[a]SEM/EDX; [b]from CO chemisorption assuming a CO:$Pt_{surface}$ stoichiometry of 0.68[1, 2]; [c]From CO chemisorption with parenthesis values from XRD via Scherrer analysis; [d]XPS; [e]N_2 BET; [f]BJH desorption isotherm

Determination of platinum oxide distribution via two different photoelectron excitation sources: a constant Pt^0 XP intensity implies homogeneous particles, a varying Pt^0 intensity implies a core-shell structure.

- The Pt^0 4f XP intensity for a 0.1 wt% Pt/SiO_2 catalyst, using Mg K_α X-rays, for which the inelastic mean free path of Pt $4f_{7/2}$ photoelectrons $\lambda_{Pt} = 1.11$ nm[3] is given by:

$$Intensity_{Pt}^{Actual\ Mg\ Ka} = Intensity_{Pt}^{Bulk\ Pt} \times exp^{-\left[\frac{(number\ of\ layers \times layer\ thickness)}{1.12}\right]} = 36.5\ arb.units$$ (experimental value)

- The Pt 4f XP intensity for a 0.1 wt% Pt/SiO_2 catalyst, using Al K_α X-rays, for which the inelastic mean free path of Pt $4f_{7/2}$ photoelectrons $\lambda_{Pt} = 1.27$ nm[3] is given by:

$$Intensity_{Pt}^{Actual\ Al\ Ka} = Intensity_{Pt}^{Bulk\ Pt} \times exp^{-\left[\frac{(number\ of\ layers \times layer\ thickness)}{1.27}\right]} = 57\ arb.units$$ (experimental value)

Since the proportion of metallic Pt is a function of escape depth, the nanoparticles most likely comprise a platinum(0) core buried beneath a capping PtO_2 film, from which the oxide film thickness may be estimated as follows:

$$\frac{Intensity_{Pt}^{Actual\ Mg\ Ka}}{Intensity_{Pt}^{Actual\ Al\ Ka}} = exp^{-\left[\frac{(number\ of\ layers \times layer\ thickness)}{1.11} - \frac{(number\ of\ layers \times layer\ thickness)}{1.27}\right]}$$

or

$$\ln\frac{36.5}{57} = -\left[\frac{(number\ of\ layers\ \times layer\ thickness)}{1.11} - \frac{(number\ of\ layers\ \times layer\ thickness)}{1.27}\right]$$

Assuming a mean PtO_2 interlayer spacing of 0.255 nm this yields:

$$\ln\frac{36.5}{57} = -\ number\ of\ layers\ x\left[\frac{(1.27 \times 0.255) - (1.11 \times 0.255)}{1.11 \times 0.255}\right]$$

which on rearrangement gives: $Number\ of\ PtO2\ layers = \frac{0.45}{0.144} = 3$

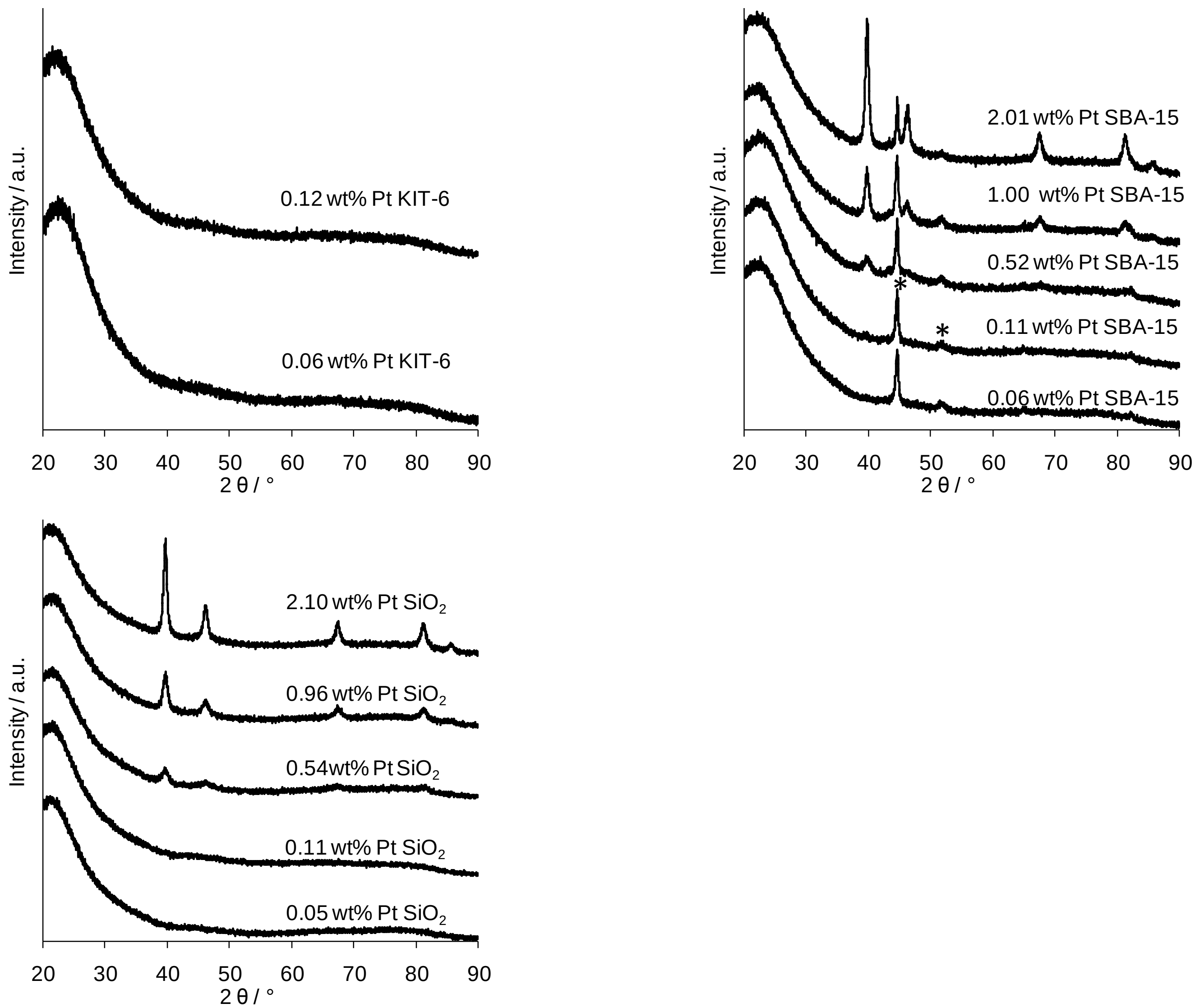

Figure S7. Wide angle XRD for Pt-impregnated KIT-6, SBA-15 and commercial fumed silica. Offset for clarity.

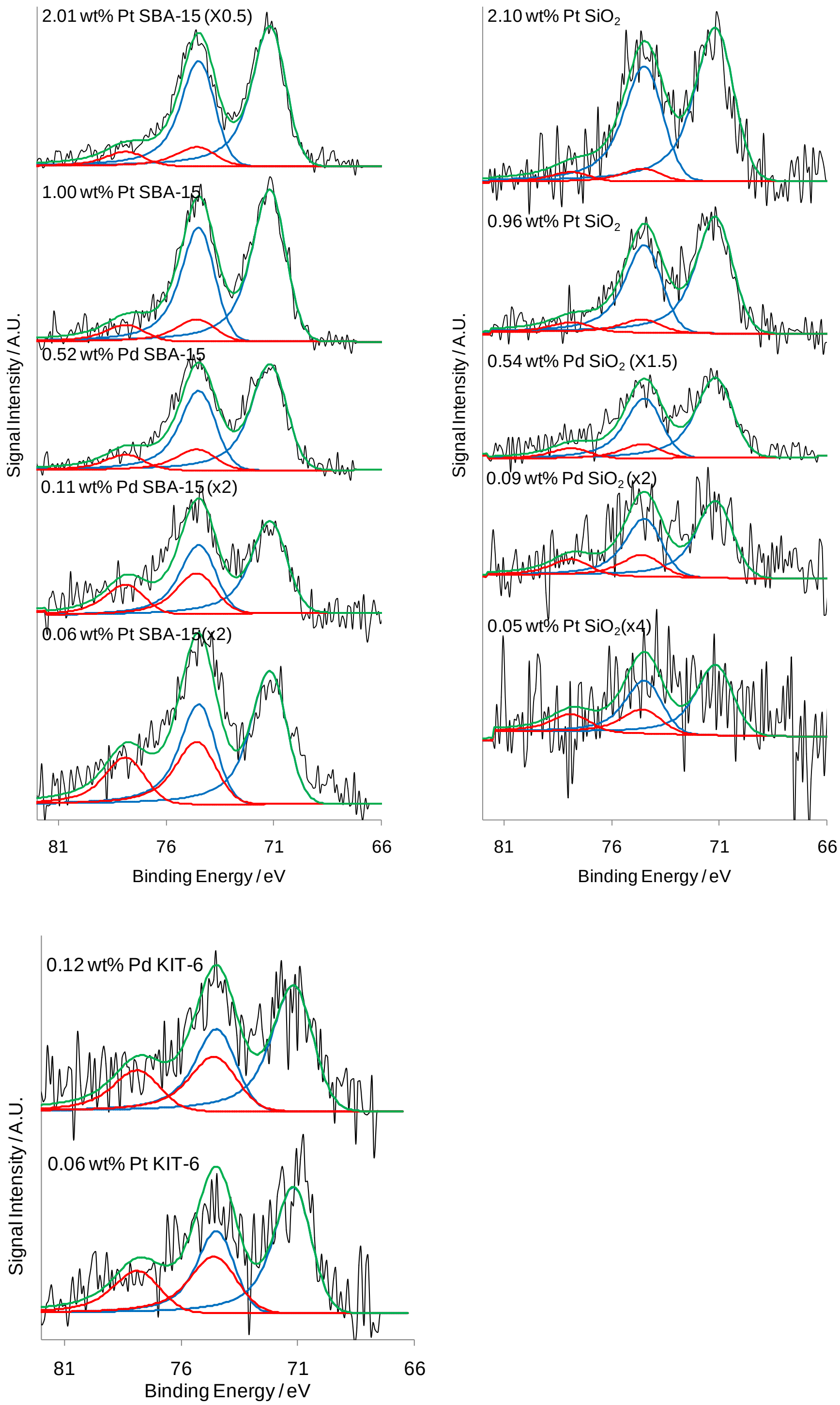

Figure S8. Fitted Pt 4f XP spectra for Pt impregnated KIT-6 (bottom), SBA-15(top left) and commercial fumed silica (top right). Offset for clarity.

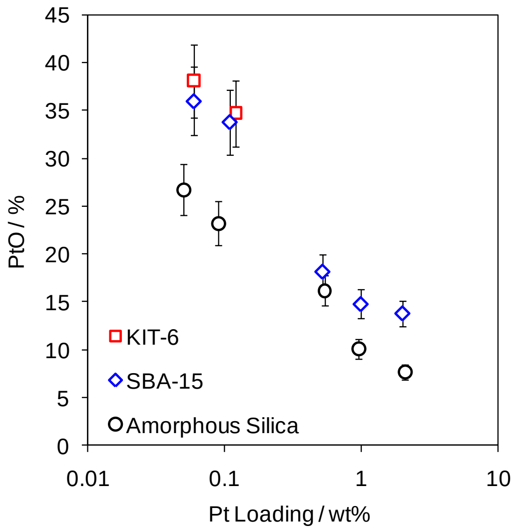

Figure S9. Effect of both metal loading and support on PtO_2 content

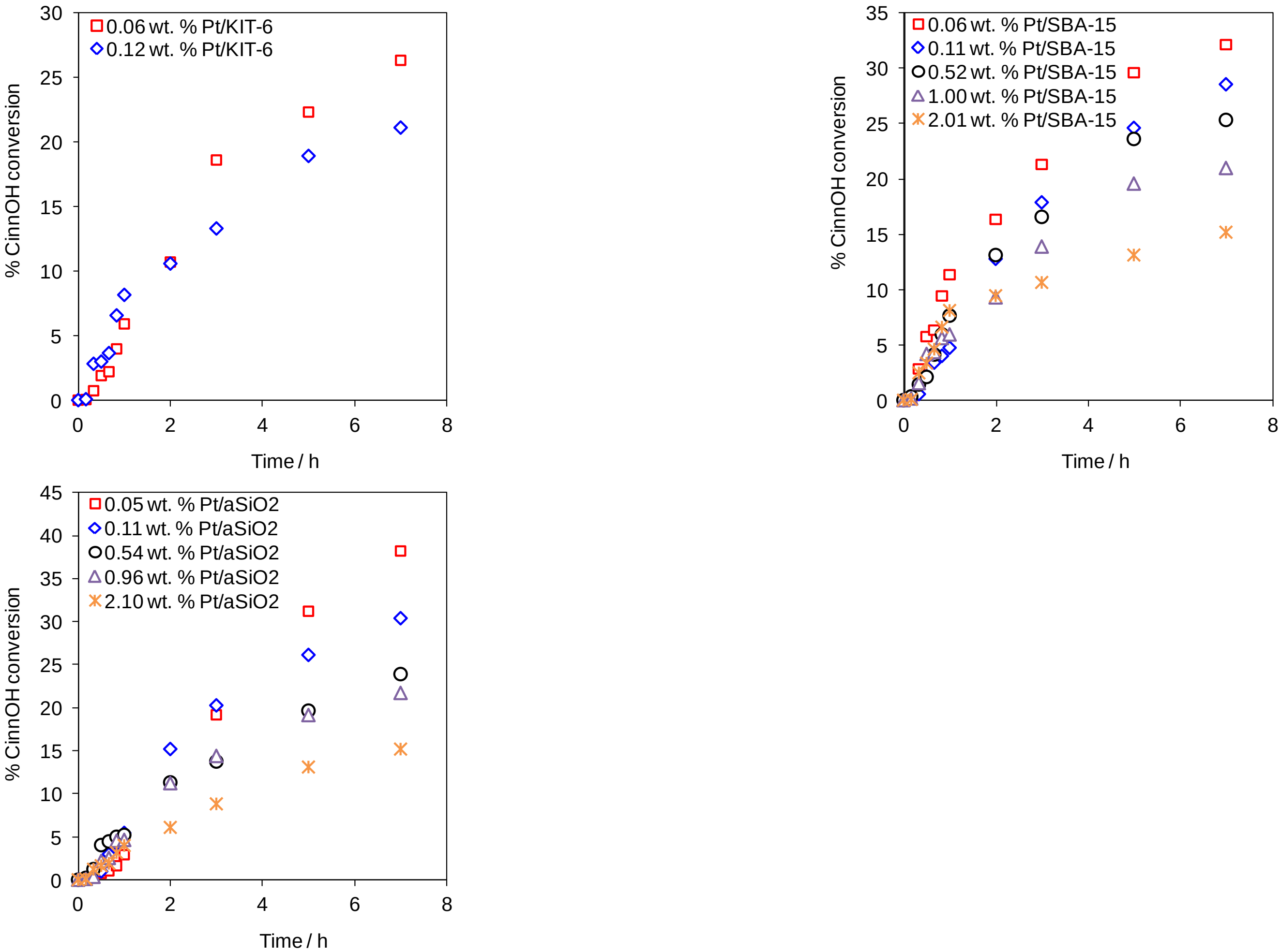

Figure S10. Cinnamyl alcohol selox reaction profiles for KIT-6 (left), SBA-15 (right) and commercial silica (bottom) series.

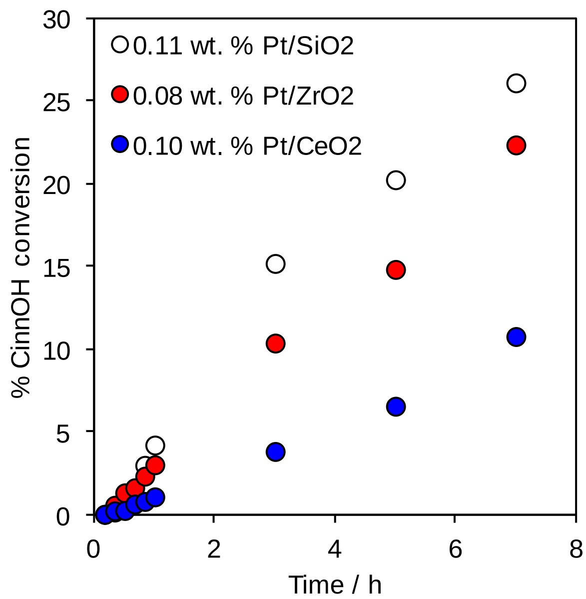

Figure S11. Cinnamyl alcohol selox reaction profiles for 0.11 wt% Pt/SiO_2 versus 0.08 wt% Pt/ZrO_2 versus 0.1 wt% Pt/CeO_2.

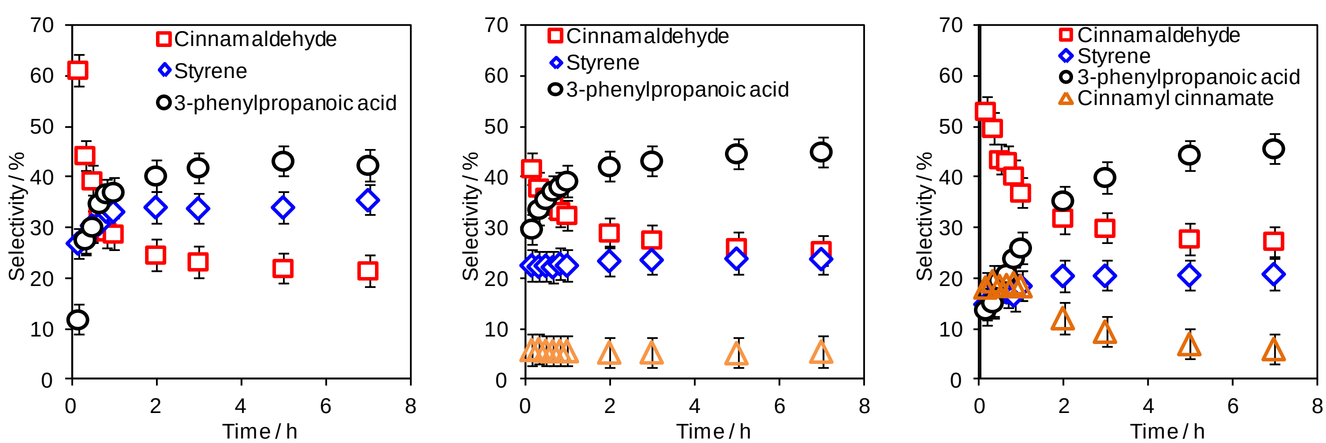

Figure S12. Selectivity profiles during cinnamyl alcohol selox over: (left) 0.11 wt% Pt/SiO_2; (middle) 0.08 wt% Pt/ZrO_2; and (right) 0.1 wt% Pt/CeO_2.

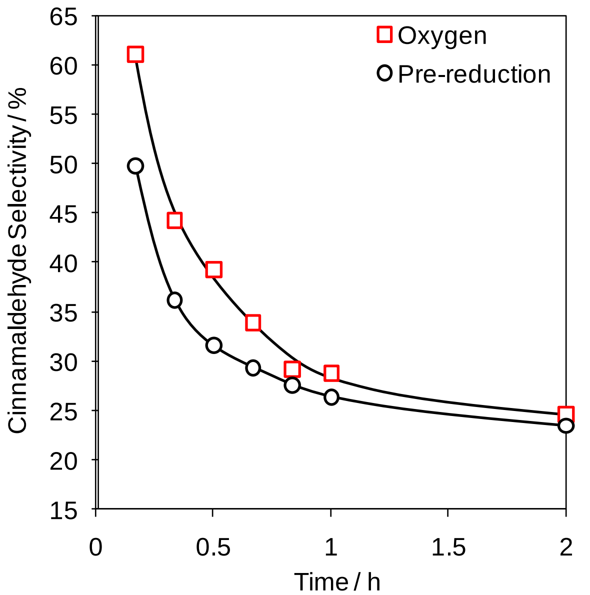

Figure S13. Effect of in-situ catalysts reduction* on 0.05 wt% Pt/SiO_2 selectivity towards cinnamaldehyde

* In situ pre-reduction protocol: Catalysts (50 mg) in toluene (7.5 mL) was treated under flowing H_2 (1 bar, 10 mL min^{-1}) at 90°C. After 1 h, the solution was purged with N_2 for 0.5 h prior to initiating reaction by addition of a solution comprising toluene (2.5 mL), mesitylene (0.1 mL), and cinnamyl alcohol (1.123 g) under flowing oxygen (5 mL min^{-1}).

1. R. Chen, Z. Chen, B. Ma, X. Hao, N. Kapur, J. Hyun, K. Cho and B. Shan, *Computational and Theoretical Chemistry*, 2012, 987, 77-83.
2. S. R. Longwitz, J. Schnadt, E. K. Vestergaard, R. T. Vang, E. Laegsgaard, I. Stensgaard, H. Brune and F. Besenbacher, *Journal of Physical Chemistry B*, 2004, 108, 14497-14502.
3. P.J.Cumpson and M.P. Seah, *Surface and Interface Analysis* **1997**, *25*, 430.